Wall temperature fluctuations measurements downstream a hydraulic pipe junction using infrared thermography

by S. Menanteau*,**, D. Bougeard*, J-L. Harion* and T. Muller**

* Ecole des Mines de Douai, EI, F-59500 Douai, France, *sebastien.menanteau@mines-douai.fr*
Univ. Lille Nord de France, F-59000 Lille, France
** AREVA NP Centre Technique, Espace Magenta, 71205 Le Creusot Cedex, France

Abstract

Thermal fatigue issue is of concern when two flows with large temperature differences are mixing. In this study, a cylindrical pipe flow comes out in a main straight channel flow through an orthogonal junction. The aim of this work is to experimentally investigate temperature fields for turbulent water flows mixing in such configurations at low velocity ratios (i.e. secondary pipe flow velocity to main flow velocity ratio). As infrared measurements are difficult to perform because of the semi-transparent properties of liquid water, we focus on the development of a specific infrared thermography procedure to get wall temperature fields in a water flow downstream the mixing region.

1. Introduction

Industrial configurations subjected to mixing process of water flows with large temperature differences are commonly used for heating or cooling purposes. Basically, two flows with different bulk velocities and temperatures, coming from a main straight pipe and a secondary one that join orthogonally, are mixed together downstream the secondary pipe exit. For flows at high Reynolds numbers and low velocity ratio V_R (defined as the ratio of the secondary pipe flow bulk velocity U_s to the main flow bulk velocity U_m), thermal stress at the wall is induced by mean and fluctuating temperatures caused by the fluid mixing and turbulence. This can eventually be the origin of cracks in the solid structure [1].

As far as thermal fatigue is concerned, most of experimental and numerical studies were carried out with two hydraulic pipes of same diameter D, Reynolds numbers varied from $Re_D=10^4$ to 10^6 (based on main bulk velocity U_m and pipe diameter) and velocity ratios varied from $V_R=0.5$ to 5 [2, 3]. A similar configuration is of interest in this paper because of the lack of data when turbulent hydraulic flows mix orthogonally at very low velocity ratios ($V_R<0.3$). In our case, main pipe diameter is larger than the secondary one so that the configuration can be seen as a plane channel flow disturbed by a smaller cylindrical jet pipe flow.

The aim of this work is to study both mean and fluctuating wall temperature induced by the mixing flow for such configurations. Different experimental tools have been previously used. For example, [4] used liquid crystal measurements to get mean wall temperature in an aeraulic junction with three rows of holes and an injection angle of 20° between the main and jet flows (V_R=1-2.5 and $Re_D=3.10^4$ - 6.10^4, based on jet pipe diameter and main velocity). They could not get access to temperature fluctuations since this technique needed a long integration time to get the steady behaviour. In other experiments, [5, 6] used infrared thermography in an aeraulic bench to study mean wall heat transfer downstream an orthogonal mixing zone with V_R varying from 1 to 5 and $Re_D=8.10^3$. They could measure wall temperature through air because of it transparent properties in the infrared wavelength range. Such measurements are not possible in hydraulic flows since water is a semi-transparent body [7, 8] in the wavelength range [3 µm; 5 µm] of the infrared camera. Therefore, direct measurements through water would only give integrated values of temperature in a volume of water of 25 µm thickness according to [9]. As it would not be representative of the wall temperature, this solution is not suitable. [10] studied turbulent water flows through a tee junction with $V_R=0.33$ and $Re_m=2.7.10^5$. They used infrared thermography to get mean and RMS temperature fields at the outer solid surface coated with a black paint and retrieved inner wall temperature with a thin layer hypothesis for the solid region (Biot number is less than 1 for the solid region). In such conditions, black coating properties and thin layer hypothesis are parameters that have to be overcome and validated to characterize temperature at the inner wall.

To get accurate mean and RMS temperature fields at the inner wall surface downstream the mixing zone in water flow, a specific infrared thermography method allowing non intrusive measurements has been developed. The infrared camera used was able to acquire snapshots at chosen frequency up to 300 Hz and could therefore give access to the fluctuating temperature signal. Investigations are made at constant velocity ratio $V_R=0.12$ and the effect of Reynolds numbers and temperature differences are studied.

2. Description of the experimental facility

The mixing of two water flows at fully turbulent regimes is studied. The cylindrical jet pipe, also called secondary pipe, has a diameter D of 20 mm. Water from the secondary pipe flows orthogonally through a main branch with Reynolds numbers varying from 3,300 to 8,300. The main branch has a rectangular section of 2D height and 7D width to ensure bi-dimensional velocity profile upstream the leading edge of the secondary pipe exit. Main flow Reynolds number

varies from 78,000 to 156,000. Figure 1 illustrates a 3D view of the experimental facility and figure 2 shows an isometric view of the mixing region.

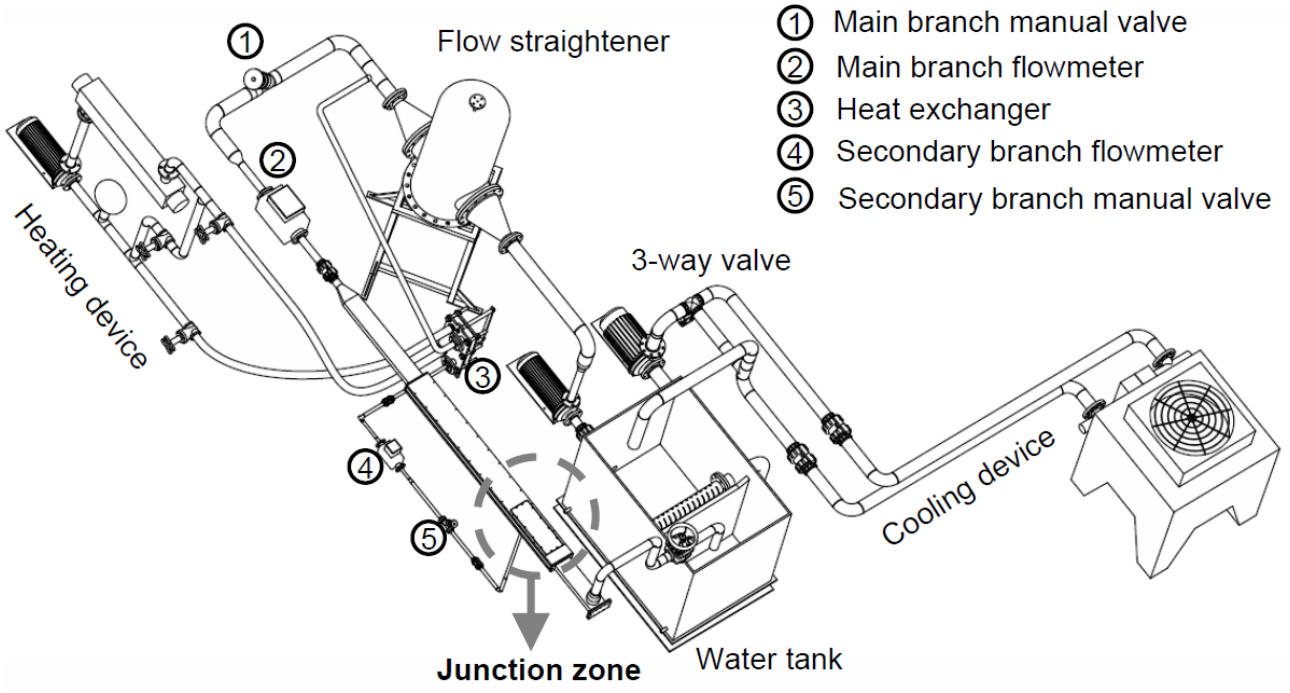

Fig. 1 *CAD view of the experimental bench*

The main and secondary flows are set with manual valves and controlled via flowmeters. A flow straightener tank prevents the main loop from being disturbed by upstream flow created by the pump. Upstream regions of the main channel and secondary pipe have been chosen long enough to create fully developed and turbulent flow at the entrance of the mixing zone. Streamwise mean and RMS (root-mean square) velocities have been measured with Laser Doppler Velocimetry (LDV) and validated in comparison with literature [11]. Considering temperature control, fluid is first taken from the water tank and cooled in a parallel loop by flowing through a cooling device regulated with an automatic 3-way valve according to the cold temperature set point T_c. The hot temperature of the jet flow is obtained via a heating device connected to a heat exchanger and allows to get a constant temperature T_h in the secondary flow.

Eventually, flows and temperatures steadiness upstream the mixing zone are controlled during the experimental measurements to ensure constant mean values. Standard deviations are always less than 1% of the mean values.

3. Infrared thermography measurements of wall temperature

3.1. Methodology

The method consists in visualizing a specific surface deposit through a transparent sapphire window in the wavelength range [3.6 µm, 5.1 µm] of the infrared camera used (short wavelength Cedip FLIR, Titanium 550M), as shown in figure 3. The interface between the fluid and the black deposit is called inner surface whereas the interface between the black deposit and the sapphire window is the outer surface.

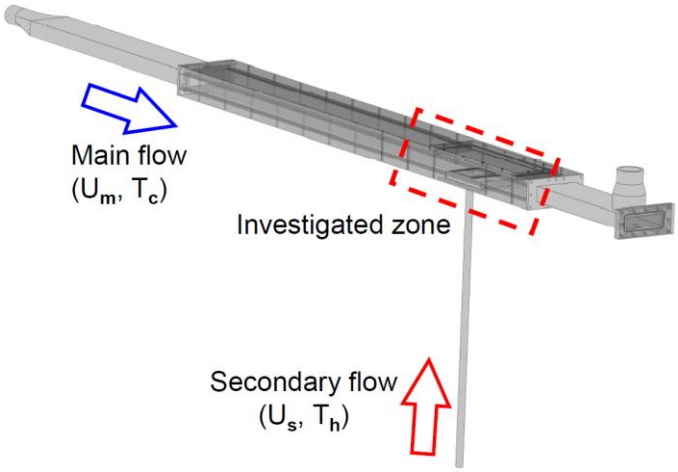

Fig. 2 *Isometric view of the designed test zone for infrared measurements*

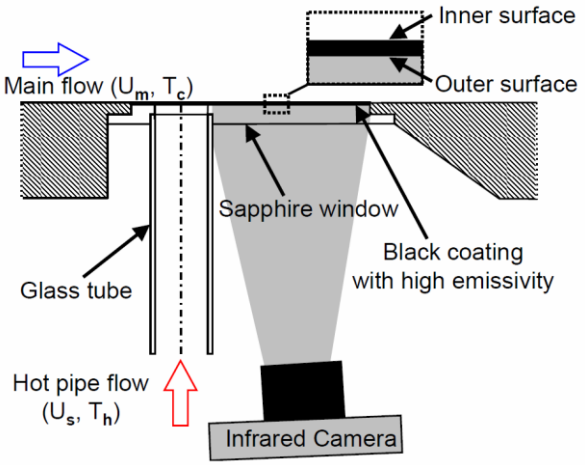

Fig. 3 *Infrared transparent window and black coating for wall temperature measurements*

The mixing flows thus impose temperature variations at the inner surface of the black coating whereas the infrared camera detects the radiative signal emitted by it outer surface. Temperature fields can eventually be determined by calibrating the digital signal of the camera according to temperature values. In order to give access to wall temperatures, the deposit must be opaque with a high emissivity value. The Fractal Coating, supplied by Acktar firm [12], has been validated with a study of the reflectivity factor which was found to be 3% by integration in the infrared bandwidth of the camera. Moreover, emissivity measurements have been made at different temperatures in comparison with a calibrated grey body (Polytec-PI/RMP SR80) and effective emissivity was found to be around 92%. Besides its radiative properties, the coating must not weaken the temperature signal from it inner surface to the outer. To this purpose, the deposit has a very small thickness of 10µm±4µm and high conductive properties (thermal conductivity given by the supplier is 50 W/m/K). Numerical investigations have shown that the coating allowed redelivery of 97% of a time variable temperature signal at 100 Hz without phase-shifting [13]. It is thus particularly efficient for such applications.

Finally, the radiative scene imaged by the infrared camera is insulated from the environment. An opaque protection has been placed around the scene and the infrared camera. A very reflective aluminum foil carefully covers the outer surface of the secondary pipe in order to prevent radiative emissions of the glass-made pipe heated by the secondary flow at T_h from being detected by the camera.

3.2. Calibration

Calibration of the infrared camera is made in-situ as it is the most efficient way to minimize environment disturbance [14, 15]: in the temperature range of $[T_c;T_h]$, the main flow is set to a constant temperature and the radiative signal is recorded by the infrared camera. 15 temperature points were used to get an interpolated polynomial of order 3 in order to convert the digital signal read from the data acquisition software into temperature values.

Before all, a non uniform correction (NUC) is made so that an offset value is added to each matrix detector of the infrared camera in order to get a uniform digital level detection. A specific post-processing method allows to remove spurious radiative signal from each instantaneous snapshot. Indeed, assuming that radiative noise created by the environment is constant during the time of acquisition, it can be removed in two steps. First, data acquisition of the wall temperature when the main and secondary flows mix is carried out (as an example, figure 4 shows an instantaneous snapshot). Secondly, the secondary pipe flow is stopped so the thermal scene is actually seen at constant temperature Tc imposed by the main flow. A mean field is obtained by recording 10 seconds of such signal, revealing the spurious signal (see figure 5). A spatial range is selected and aims to represent the unaffected part of the thermal scene (outlined in figure 5). Eventually, the mean spurious signal is subtracted from each instantaneous snapshot and an offset value corresponding to the mean value obtained in the selected zone is added. Spatial variations of the spurious signal is thus taken into consideration and removed from the thermal field.

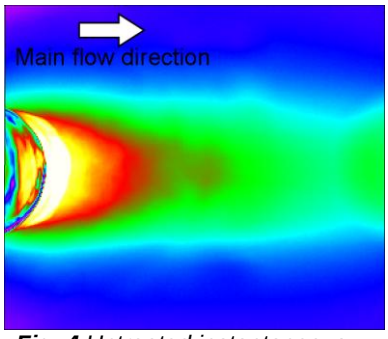

Fig. 4 *Untreated instantaneous snapshot of digital level*

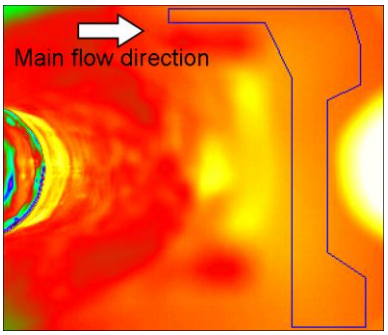

Fig. 5 *Mean digital level values obtained at constant temperature*

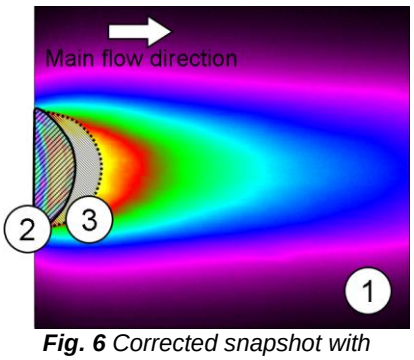

Fig. 6 *Corrected snapshot with spurious signal removal*

Nevertheless, all cautions taken do not yet prevent the surface seen by the camera from being affected by some residual noise. Figure 6 gives an example of spurious radiation regions, namely 2 and 3, which are interpreted through figure 7. The numbered 2 radiative signal comes from direct view of the glass-made pipe covered with aluminum foil. Signal 3 is emitted from the glass pipe toward the outer surface of the black deposit and then reflected toward the infrared camera. Eventually, this gives an 8 mm loss of signal downstream the trailing edge of the pipe exit. In the following, the altered regions will be hatched in figures representing spatial mean and RMS fields.

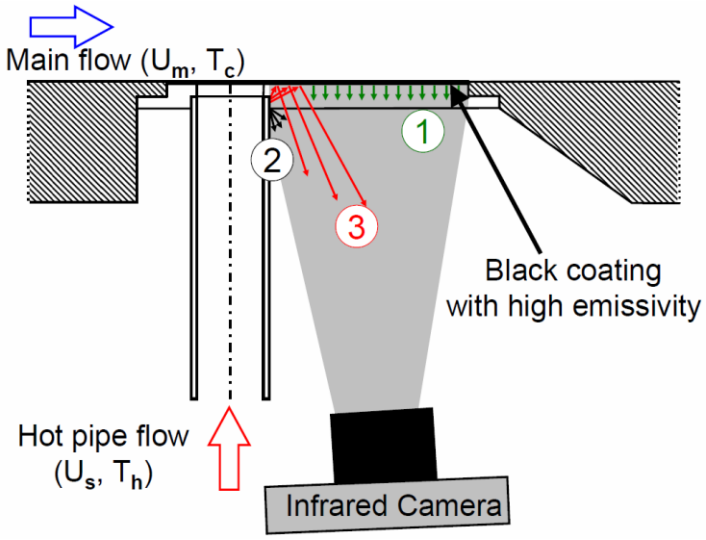

Fig. 7 *Signal detection of the infrared camera*

3.3. Error and uncertainty estimations

Even though a specific care has been made to calibrate the infrared camera, experimental errors and uncertainties still remain. These can be estimated with the knowledge of:

- The error and uncertainty due to the thermal probe used as reference to calibrate platinum probes. These values can be estimated from the supplier certificate,
- The error and uncertainty caused by the interpolation law used to get fluid temperatures from the probes upstream the mixing zone,
- The error and uncertainty caused by the interpolation law obtained to get temperatures from digital level given by the infrared camera,
- The uncertainty due to the infrared sensor noise of the camera, known as noise equivalent temperature difference (NETD).

Finally, global error is obtained by summing the errors while global uncertainty is found by taking the mean square root of the sum of the squared uncertainties [16]. Mean error and uncertainty were found to be 0.062°C and 0.42°C respectively, in the temperature range [29°C;45°C]. One can notice that uncertainty on the data is quite high. This is mainly due to the reference probe uncertainty values that range from 0.3°C at 0.07°C 0.6°C at 100.01°C.

As far as temperature fluctuations uncertainty is concerned, the NETD value is only taken into consideration so that uncertainty is 0.055°C.

Eventually, the infrared camera owns a matrix of 320x256 detectors, giving a spatial resolution of 0.22 mm per pixel for the radiative scene observed.

4. Results

Based on the work of [17, 18], a Wiener filter has been applied on the 2D field values to get smoothed plots as it is specifically convenient for infrared thermography data. The Wiener filter is a non-uniform spatial filter that operates on the data like a smooth filter where the signal to noise ratio is low and does not affect data where the signal to noise ratio is high.

Mean and RMS fields presented below are normalized with the following relations:

$$\overline{T}^* = \frac{\overline{T} - T_c}{T_h - T_c}$$

$$T^*_{rms} = \frac{T_{rms}}{T_h - T_c}$$

Eventually, 26,000 snapshots are recorded to ensure statistical convergence of mean and RMS values (acquisition duration varied from 17'20s at 25 Hz to 2'10s at 200 Hz).

4.1. Influence of camera parameters

A first investigation about infrared camera parameters is carried out to check whether the results show dependency of the data acquisition frequency and the integration time of the InSB detectors.

Snapshots are recorded and processed at 25 Hz and 200 Hz by the infrared camera for a fixed flow configuration with V_R=0.12, Re_m=78,000 and T_h-T_c=15°C. Figure 8 shows radial profiles of dimensionless mean temperature plotted at several distances from the centre of the secondary pipe exit (these radial profiles are illustrated in figures 12 and 13). Mean values tend to decrease as the profile is extracted far from the pipe exit, revealing the mixing behaviour between the hot and cold flows. Besides, mean profiles are identical whatever the data acquisition frequency used. Figure 9 shows radial profiles for dimensionless RMS temperature. Two peaks of high RMS values are located on both sides downstream the pipe exit and fluctuation values vanish further downstream. Again, data obtained at 25 Hz and 200 Hz show good agreement.

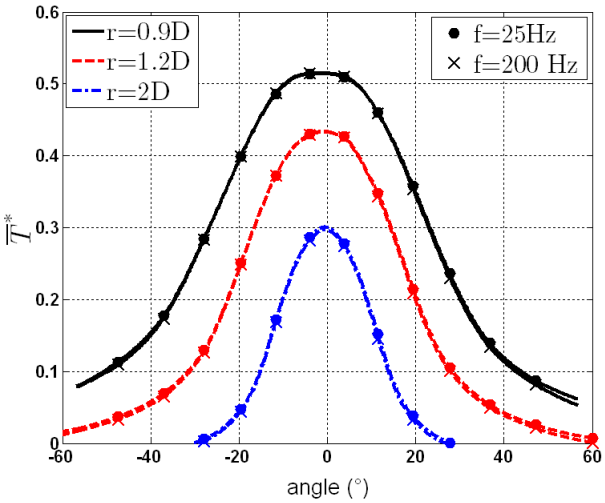

***Fig. 8** Plot of dimensionless mean temperature for V_R=0.12 and Re_m=78,000*

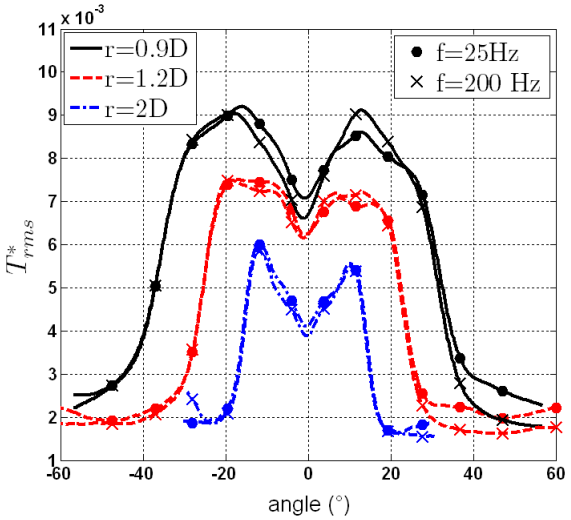

***Fig. 9** Plot of dimensionless RMS temperature for V_R=0.12 and Re_m=78,000*

Another camera parameter that has to be checked is the time exposure of the InSb detectors during measurements. The longer detectors are exposed to the radiative signal coming from the thermal scene, the more sensitive and accurate they are but the narrower the temperature range of detection is. A compromise has thus to be found for this parameter. The study is made with V_R=0.12, Re_m=78,000 and T_h-T_c=5°C. The small temperature difference used allows to select two integration time, 1350 µs and 1800 µs.

Figure 10 presents normalized mean temperature profiles. Comparison shows good agreement between the two sets of data. When comparing RMS values in figure 11, signal to noise ratio varied for the two time exposures thus creating a shift between the weakest values. In order to overcome the signal to noise ratio difference due to the detector sensitivity, an offset value set to the minimum of RMS has been subtracted. As this change is arbitrary, no value has been put in vertical scale in figure 11 but one can observe the good agreement between plots. Besides, measured RMS values are of the order of the detection limit of the infrared camera given by the NETD; noise created by the detector sensitivity can explain the small discrepancies observed for plots at r=1.2D and r=2D.

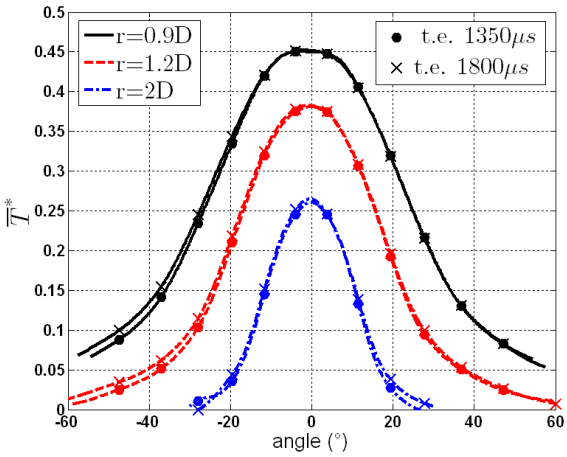

Fig. 10 *Plot of dimensionless mean temperature for V_R=0.12 and Re_m=78,000*

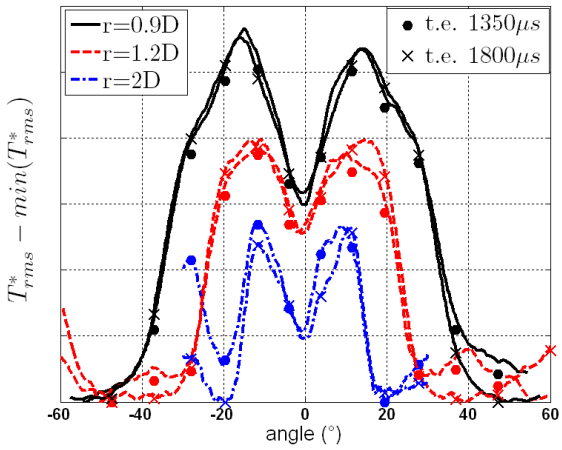

Fig. 11 *Plot of dimensionless RMS temperature for V_R=0.12 and Re_m=78,000*

This study thus shows that camera parameters effects on temperature fields are of small importance. In the next section, influence of flow conditions on temperature fields is analysed.

4.2. Influence of flow conditions

In orthogonal junction pipes, coherent structures of the mean dynamic flow have been widely studied for velocity ratios greater than 0.5 [19, 20]. As far as configurations at low velocity ratios and high Reynolds numbers are concerned, only a few articles deal with dynamic analysis. [21, 22] studied jet in crossflow for Re_D=400,000 (based on the free stream velocity above a flat plate and the jet pipe diameter) and V_R=0.1 with Large Eddy Simulation. They pointed out the formation of a counter-rotating vortex pair (CVP) in the wake region. It was also observed a vortex inside the jet pipe formed by the blocking effect of the main flow at the leading edge of the pipe exit. It was found to convect along the wall inside the pipe and to catch up with the wake region further downstream. A reverse flow was also observed in the wake region. Eventually, a shear layer appeared above the CVP and the inferior part of the CVP remained along the wall due to the weak depth penetration of the jet pipe in the main flow. Such flow behaviours were also identified in [13] and are of interest when trying to qualitatively explain wall mean and fluctuating temperature behaviours.

4.2.1. Influence of temperature difference between hot and cold flows at the entrance of the mixing zone

In this section, flow configuration is set to V_R=0.12 and Re_m=78,000 and temperature differences between hot and cold flows are compared. As an example, figure 12 shows the normalized mean wall temperature field measured for V_R=0.12, Re_m=78,000 and T_h-T_c=15°C. Near the pipe exit, the highest temperature values are found. Then, they decrease with downstream distance. The thermal wake region is narrow in the spanwise direction (z direction) indicating the local behaviour of mixing process at the wall. From the knowledge of the flow behaviour briefly described previously, it can be pointed out that the weak depth penetration of the pipe flow into the main stream may cause the small spanwise extension of the mixing process, whereas the streamwise reverse flow in the wake [22] may explain the weak mixing property near the pipe exit.

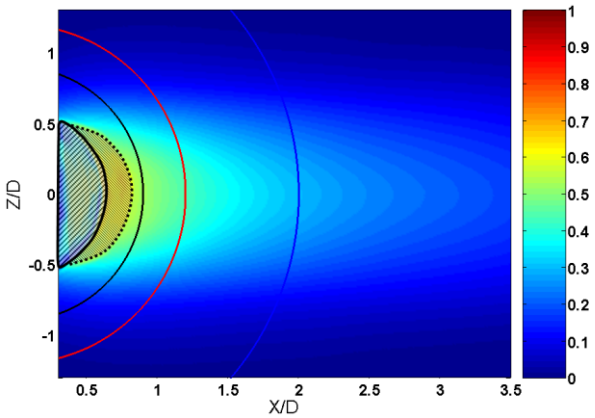

Fig. 12 Dimensionless m*ean wall temperature obtained for velocity ratios V_R=0.12 and Re_m=78,000*

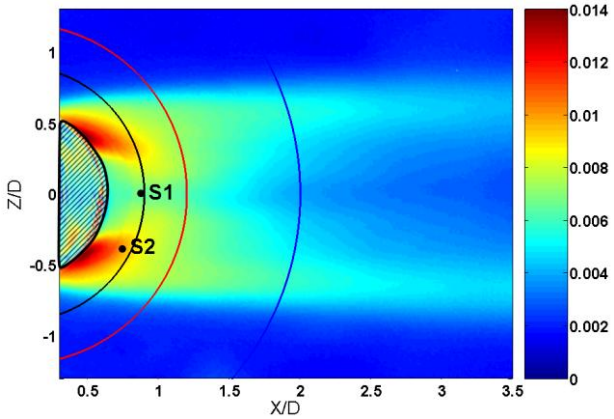

Fig. 13 Dimensionless RMS *wall temperature fluctuations obtained for velocity ratios V_R=0.12 and Re_m=78,000*

Figure 13 shows the dimensionless RMS temperature field. It reveals two maxima of high RMS values that are located on both sides of the pipe exit and progressively dissipate further downstream. These regions of greatest temperature fluctuations can be related to turbulence mechanisms in the wake region. At the trailing edge of the pipe exit, a vortex pair forms and induces flow turbulence that can be deemed the origin of wall temperature fluctuations.

Effects of temperature difference are then observed in the spectral domain. Power spectral density (PSD^*) is obtained with dimensionless temperature and then normalized with U_m/D and is presented in figures 14 and 15 for two probes located in figure 13. Extracted temporal signals have been divided in 1024 samples on which a fast fourier transform method has been applied. 47 spectra have thus been averaged to get mean tendencies. In figures 14 and 15, frequency is presented as a Strouhal number defined with U_m and D. For each case investigated, spectra show the same slope tendencies. Further investigations have been undertaken on other probe locations and give the same results.

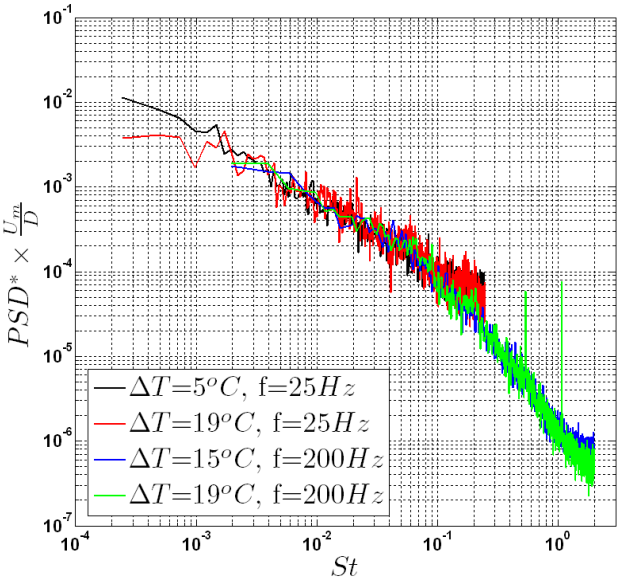

Fig. 14 *Plots of PSD for 3 temperature differences and at 2 frequency acquisitions of the infrared camera - Probe 1*

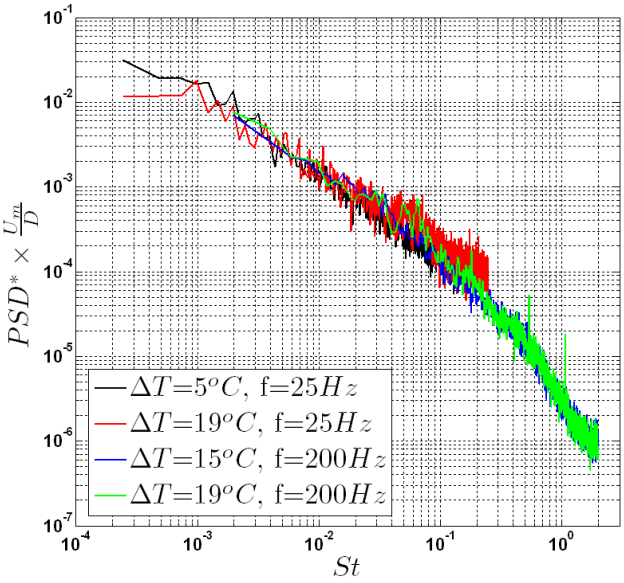

Fig. 15 *Plots of PSD for 3 temperature differences and at 2 frequency acquisitions of the infrared camera - Probe 2*

From this study, it can be seen that once normalized, temperature differences between hot and cold flows do not seem to have any effect on wall temperatures.

4.2.2. Influence of Reynolds number

In this section, mixing flow at two Reynolds numbers Re_m=78,000 and 156,000 are investigated while both velocity ratio and temperature difference are kept constant (VR=0.12 and Th-Tc=15°C). 2D mean and RMS fields for Re_m=78,000 have been previously presented in figures 12 and 13, and figures 16 and 17 respectively show the mean and RMS normalized temperature fields for Re_m=156,000.

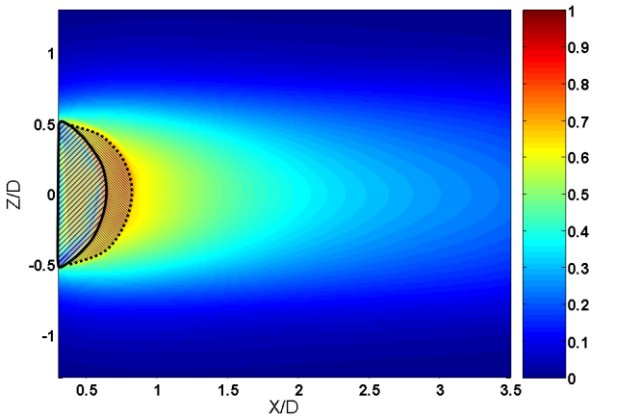

Fig. 16 Dimensionless m*ean wall temperature obtained for velocity ratio V_R=0.12 and Re_m=156,000*

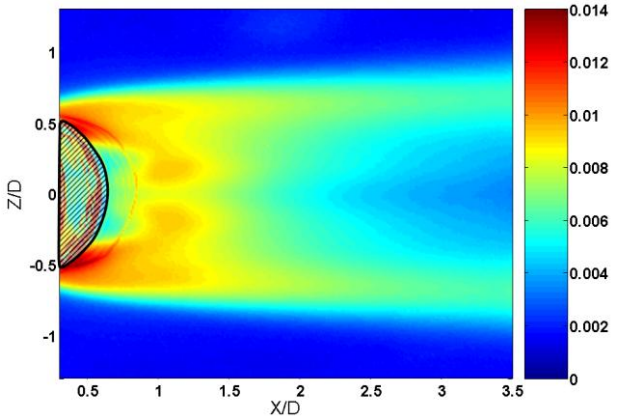

Fig. 17 Dimensionless *RMS wall temperature obtained for velocity ratio V_R=0.12 and Re_m=156,000*

The evolution of the mean temperature field is similar in both cases. When comparing radial plots extracted at several positions (see figure 18), it can be observed that temperature values are higher for the higher investigated Reynolds number.

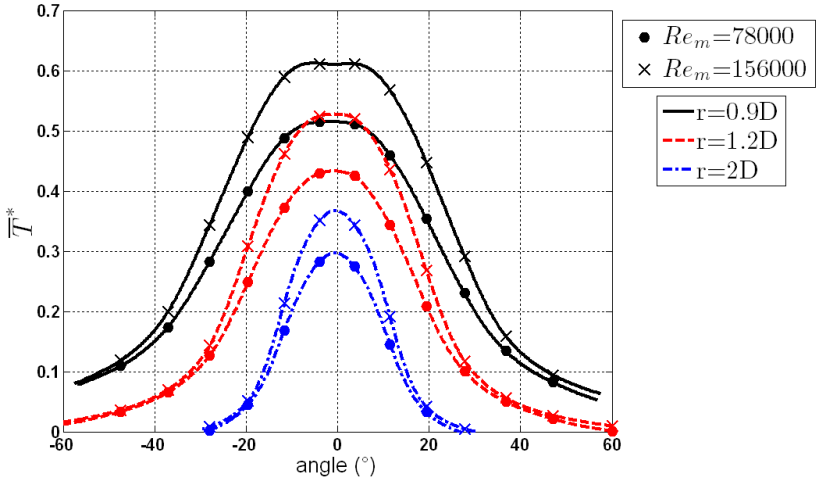

Fig. 18 *Comparison of dimensionless mean temperature plots for Re_m=78,000 and 156,000*

Moreover, although highest values of RMS fields are of the same order in both cases (figures 13 and 17), spatial distributions are quite different. Peaks of high RMS values are observable on both sides of the pipe exit but dissipation of fluctuation seems stronger further downstream in the case Re_m=78,000. Radial profiles of RMS fields are plotted in figure 19. For plots at r=0.9D, highest values are similar for both cases. On the other hand, at r=1.2D and r=2D, temperature fluctuations are greater for Re_m=156,000.

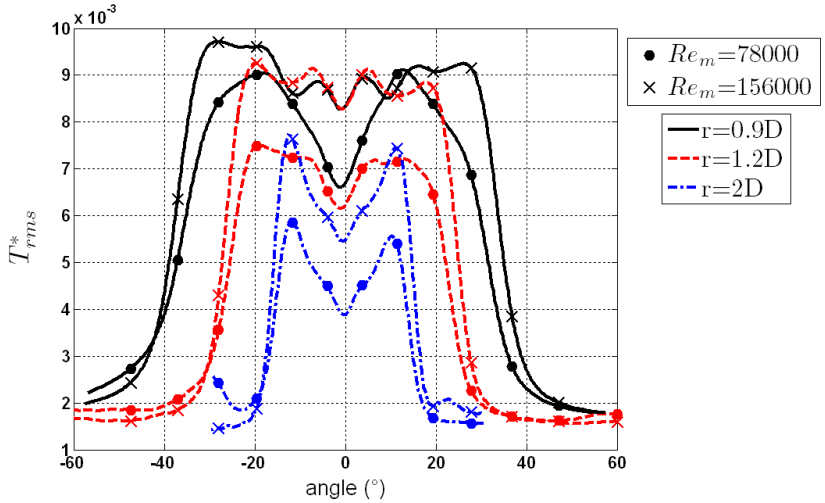

Fig. 19 *Comparison of dimensionless RMS temperature plots for Re_m=78,000 and 156,000*

An explanation of such modifications can be qualitatively given when considering a flow developing on a plane plate; increasing the Reynolds number induces a reduction of wall viscous sub-layer which acts like a low-pass filter on temperatures. Wall surface is thus impacted more strongly by fluid temperature from the dynamic structures convecting nearby. In our case, this mechanism can be observed in the wake with the reduction of the boundary layer because of the increase of Reynolds number. This phenomenon may be the reason of mean and RMS fields modifications, all the more so as vortex structures formed in the wake region may have strong effect on thermal transport and wall temperature.

5. Conclusion

Experimental mean and RMS temperature fields have been obtained at the wall of a hydraulic flow mixing in an orthogonal junction with fully turbulent conditions and low velocity ratios. Investigations have been carried out using

infrared thermography and a specific opaque and high emissive coating at the interface between fluid and solid regions has been validated to get accurate temporal and spatial wall measurements. Spatial and temporal data have thus been obtained, allowing access of complete information of both mean and fluctuating wall temperature fields.

For a given configuration, we first compare infrared measurements obtained for two acquisition frequencies and then two different integration times. Results are found to be independent of these camera parameters and the analysis of the influence of flow conditions was undertaken. Temperature differences imposed between the hot and cold flows at the entrance of the mixing area show no effect when comparing normalized spectra of temperature. Then, influence of Reynolds number on wall temperature has been carried out. Normalized mean temperature fields show the same trends for both cases with the highest values near the trailing edge of the pipe exit that decrease due to the mix of the main and secondary flows. In the wake region, mean values are always higher for the higher Reynolds number case, however. RMS temperature fields have then been compared. Although highest RMS temperature values are similar in both cases, discrepancies between spatial behaviours are observed. These modifications in fluctuation distributions may be caused by the reduction of the dynamic viscous sub-layer thickness with the increase of the Reynolds number, which consequently changes heat transfer in the vicinity of the wall.

Acknowledgments

The authors would like to thank AREVA technical centre of Le Creusot for their helpful support, collaboration and useful discussions.

REFERENCES

[1] Chapuliot S., Gourdin C., Payen T., Magnaud J.P. and Monavon A., “Hydro-thermal-mechanical analysis of thermal fatigue in a mixing tee”. Nuclear Engineering and Design, vol. 235(5), pp. 575–596, 2005.
[2] Benhamadouche S., Sakiz M., Péniguel C. and Stephan J-M., “Presentation of a new methodology of chained computations using 3D approaches for the determination of thermal fatigue in a T-junction of a PWR nuclear plant”. 17th International conference on Structural Mechanics in Reactor Technology, SMiRT 17, Prague (Czech Republic), 2003.
[3] Jayaraju S.T., Komen E.M.J. and Baglietto E., “Suitability of wall-functions in large eddy simulation for thermal fatigue in a T-junction”. Nuclear Engineering and Design, In Press, Corrected Proof, 2010.
[4] Ou S. and Rivir R. B., “Leading edge film cooling heat transfer with high free stream turbulence using a transient liquid crystal image method”. International Journal of Heat and Fluid Flow, vol. 22(6), pp. 614–623, 2001.
[5] Carlomagno G.M., Nese F.G., Cardone G. and Astarita T., “Thermo-fluid-dynamics of a complex fluid flow”. Infrared Physics & Technology, vol. 46(1-2), pp. 31–39, 2004.
[6] Carlomagno G.M., “Colours in a complex fluid flow”. Optics & Laser Technology, vol. 38(4-6), pp. 230–242, 2006.
[7] Segelstein D.J., “The complex refractive index of water”. PhD, University of Missouri, Kansas City, 1981.
[8] Zolotarev V.M., Mikhilov B.A., Alperovich L.L. and Popov S.I., “Dispersion and absorption of liquid water in the infrared and radio regions of the spectrum”. Optics and Spectroscopy, vol. 27, pp. 430–432, 1969.
[9] Volino R.J. and Smith G.B., “Use of simultaneous IR temperature measurements and DPIV to investigate thermal plumes in a thick layer cooled from above”. Experiments in Fluids, vol.27, pp. 70–78, 1999.
[10] Kuhn S., Braillard O., Niceno B. and Prasser H.-M., “Computational study of conjugate heat transfer in T-junctions”. Nuclear Engineering and Design, vol. 240(6), pp. 1548–1557, 2010.
[11] Abe H., Kawamura H. and Matsuo Y., “Surface heat-flux fluctuations in a turbulent channel flow up to Re_=1020 with Pr=0.025 and 0.71. International Journal of Heat and Fluid Flow, vol. 25(3), pp. 404–419, 2004.
[12] Acktar Advanced coatings, website: www.acktar.com/category/FractalBlack
[13] Menanteau S., “Etude expérimentale et numérique des fluctuations de température en aval d’une jonction orthogonale d’écoulements turbulents de températures différentes”. PhD, Ecole des Mines de Douai and Université de Valenciennes et du Hainault-Cambrésis, France, 2012.
[14] Pajani D., “Mesures par thermographie infrarouge”. A ed., 1989.
[15] Minkina W. and Babka R., “Influence of components of the error of method on error of temperature indication on the basis of the thermacam pm595 infrared camera measurement model”. In B. Wiecek, ed. Proceedings of V national conference, thermography and thermometry in infrared, vol.14-16, pp. 339–344, 2002.
[16] Moffat R.J., “Describing the uncertainties in experimental results”. Experimental Thermal and Fluid Science, vol. 1(1), pp. 3–17, 1988.
[17] Rainieri S. and Pagliarini G., “Data filtering applied to infrared thermographic measurements intended for the estimation of local heat transfer coefficient”. Experimental Thermal and Fluid Science, vol. 26(2-4), pp. 109–114, 2002.
[18] Rainieri S., Bozzoli F. and Pagliarini G., “Wiener filtering technique applied to thermographic data reduction intended for the estimation of plate fins performance”. Experimental Thermal and Fluid Science, vol. 28(2-3), pp. 179–183, 2004.
[19] Kelso R.M., Lim T.T. and Perry A.E., “An experimental study of round jets in cross-flow”. Journal of Fluid Mechanic, vol. 306, pp. 111–144, 1996.
[20] Fric T.F. and Roshko A., “Vortical structure in the wake of a transverse jet”. Journal of Fluid Mechanics, vol. 279, pp.1–47, 1994.

[21] Guo X., Schroder W. and Meinke M., “Large-eddy simulation of film cooling”. Proceedings of the Int. Gas Turbine Congress, Tokyo (Japan), 2003.
[22] Guo X., Schroder W. and Meinke M., “Large-eddy simulations of film cooling flows”. Computers & Fluids, vol. 35(6), pp. 587–606, 2006.